

PROCEEDINGS OF SPIE

[SPIDigitalLibrary.org/conference-proceedings-of-spie](https://spiedigitallibrary.org/conference-proceedings-of-spie)

Optofluidics

David Erickson, Xin Heng, Zhenyu Li, Troy Rockwood,
Teresa Emery, et al.

David Erickson, Xin Heng, Zhenyu Li, Troy Rockwood, Teresa Emery,
Zhaoyu Zhang, Axel Scherer, Changhui Yang, Demetri Psaltis,
"Optofluidics," Proc. SPIE 5908, Optical Information Systems III, 59080S (10
September 2005); doi: 10.1117/12.623629

SPIE.

Event: Optics and Photonics 2005, 2005, San Diego, California, United States

Optofluidics

David Erickson^{*}, Xin Heng, Zhenyu Li, Troy Rockwood, Teresa Emery, Zhaoyu Zhang,
Axel Scherer, Changhuei Yang and Demetri Psaltis^{**}
Center for Optofluidic Integration, California Institute of Technology, Pasadena, California, 91106

ABSTRACT

“Optofluidics” is the marriage of optics, optoelectronics and nanophotonics with fluidics. Such integration represents a new approach for dynamic manipulation of optical properties at length scales both greater than and smaller than the wavelength of light with applications ranging from reconfigurable photonic circuits to fluidically adaptable optics to high sensitivity bio-detection currently under development. The capabilities in terms of fluidic control, mixing, miniaturization and optical property tuning afforded by micro-, nano- and electro-fluidics combined with soft lithography based fabrication provides an ideal platform upon which to build such devices. In this paper we provide a general overview of some of the important issues related to the fabrication, integration and operation of optofluidic devices and present three comprehensive application examples: nanofluidically tunable photonic crystals, optofluidic microscopy and DFB dye lasers.

Keywords: Optofluidics, Optics, Photonics, Nanophotonics, Nanofluidics, Photonic Crystal, Dye Laser, Microscopy, Biophotonics.

1. Introduction

The concept behind optical devices which incorporate liquids as a fundamental part of the optical structure can be traced at least as far back as the 18th century where rotating pools of mercury were proposed as a simple technique to create smooth spherical mirrors for use in reflecting telescopes¹. Modern microfluidics^{2,3} has enabled the development of a present day equivalent of such devices which we refer to as “Optofluidics.” Some of the more prominent examples of such devices include: liquid crystal infused photonic crystal lasers⁴, fluid-fluid waveguides⁵ and florescent light sources⁶, polarization independent fluidic switches⁷, microfluidically tuned optical fibers^{8,9} and inteferometers¹⁰, and electrowetting based adaptable fluidic lenses¹¹ and electronic paper¹². In this paper we will give a brief overview of some basic microfluid dynamics focusing on issues relevant to the operation of optofluidic devices. The final section, comprising the bulk of this paper, will comprise of three illustrative examples of optofluidic projects currently under development, namely sub-wavelength scale tuning of photonic crystals, ultra small fluidic imaging devices and soft elastomer based distributed feedback dye lasers. We begin however with an overview of the advantages of optofluidics along with a selection of some of the major applications.

1.1. Adaptive and reconfigurable optical systems

A key factor for high performance adaptive optical system is the capability to dynamically control either the physical layout or the refractive indices of the optical components. Recent advancements in optical MEMS technology¹³ has provided significant functionality and flexibility to the former of these (*e.g.* optical switching and reconfigurable mirror arrays). Traditional techniques for manipulating the refractive index through the application of electric, acoustic or mechanical strain fields are limited in this respect by the achievable $\Delta n/n$, as is shown in Table 1.1. Optofluidics offers an order of magnitude jump in this quantity allowing for the development of an entirely new class of adaptive optical system in which, when combined with soft lithography based nanofluidics, the index of refraction can in principal be arbitrarily reconfigured at scales significantly smaller than the wavelength of light (in section 3.1 we will demonstrate the use of nanofluidics to address a single row of holes within a two dimensional photonic crystal). At present modulation speeds for such tuning can be in the millisecond range but are ultimately limited by the viscous nature of the

^{*} Present Address: Department of Mechanical and Aerospace Engineering, Cornell University, Ithaca, NY

^{**} Corresponding author: D. P., E-mail: psaltis@optics.caltech.edu

process and the mechanical actuation techniques that are popularly used. As will be discussed in section 2.2, alternative transport mechanisms such as electrokinetics could serve to reduce the time response even further, though likely not to the scale required for high speed optical switching applications.

Table 1.1: Comparison of optofluidics with traditional optical tuning techniques

Technology	O($\Delta n/n$)	Time response (s)
Optofluidics	1	10⁻³
Liquid crystal	0.1	10 ⁻³
Injection current	0.02	10 ⁻⁹
Temperature	0.02	1
Photorefractive	0.001	10 ⁻¹ -10 ⁻⁵
Electrooptic (10 kV/cm)	0.002	10 ⁻¹²
Photoelastic/ Acoustooptic (10W)	0.0001	10 ⁻⁶ -10 ⁻⁷

1.2. Optofluidic Biosensors

The integration of microfluidics with optical detection techniques has been a field of active interest for several years (see Prasad¹⁴ for an overview of optical biosensors and Erickson and Li¹⁵ for an overview of integrated microfluidic devices). In addition to traditional fluorescence based detection, techniques relying on the incorporation of planar waveguides, evanescent wave fields or surface plasmons are particularly suitable for integration with microfluidics. While such techniques have proven exceptionally successful, a particularly fruitful path for future research in optofluidics is in the development of resonant cavity sensors. Such sensors can take advantage of the extremely high quality factor to mode volume ratios (Q/V) achieved in nanophotonic structures¹⁶ to perform single or few molecule sensing. The challenges here will be to not only develop techniques for delivering, attracting or concentrating bioentities into the resonant cavities, but being able to perform highly specific detection as well.

1.3. Thermal Stabilization

The incorporation of liquids directly into the optical structure also has inherent advantages in terms of temperature stabilization. In general the heat transfer coefficient (which is the proportionality constant between heat rejection and surface temperature) for systems immersed in air ranges from 10 W/m²K to 100 W/m²K, depending strongly on the geometry and flow velocity. As a result of the higher density, specific heat capacity and thermal conductivity of water immersed systems, heat transfer coefficients typically range from 500 W/m²K to 10,000 W/m²K thus representing at least an order of magnitude decrease in the temperature rise for a given heat rejection requirement. It is important to note that while this represents a general rule for global heat transfer, more detailed modeling is required to accurately predict the local heat transfer enhancement.

2. Optofluid dynamics

In the broadest sense, optofluidics involves the manipulation of the optical properties of a system using fluidics and conversely the manipulation of fluidic properties of a system with optics. It is thus inherently concerned with both the optical and thermophysical properties of the fluid and the dynamics of how both the optical and flow fields change in response to external stimuli. In this section we will provide a brief overview of some of the fluids of particular interest in optofluidics and some of their important optical and thermophysical properties. The following subsection will provide a brief overview of the relevant microfluid dynamics with a focus on the issues of relevance to optofluidics.

2.1. Optofluids

Table 2.1 provides an overview of a small sampling of liquids of the relevant properties for a few common optofluidic liquids. Note that this represents a non-comprehensive list, other parameters of particular interest include: fluid-fluid surface tension, fluid-solid surface energy, contact angle, fluid-solid electroosmotic mobility, compatibility with soft elastomers²⁰ and numerous others.

Table 2.1: Some fluids used in optofluidic devices*

Fluid	Optical Properties			Thermophysical Properties		
	Refractive index, n	Temperature derivative, dn/dT (10^{-4} 1/K)	Non-linear refractive index, γ (10^{-20} m ² /W)	Viscosity, η (mPa s)	Density, ρ (kg/m ³)	Thermal conductivity, k (W/m K)
Water, H ₂ O	1.33299 ¹⁷	-0.8 ¹⁷	2.7 ^{b, 17}	0.890 ¹⁷	997.05 ¹⁷	0.6071 ¹⁷
Heavy Water, D ₂ O	1.32828	-	6.4 ^{c, 17}	-	1104.4 ¹⁷	-
Methanol, CH ₄ O	1.33118 ¹⁷	-4.68 ^{a, 17}	4.7 ^{b, 17}	0.544 ¹⁷	787.2 ¹⁷	0.200 ¹⁷
5.03M Aqueous CaCl ₂	1.4420 ¹⁸	-	-	8.997 ¹⁸	1395.7 ¹⁸	-
Ethylene glycol, C ₂ H ₆ O ₂	1.4318 ¹⁷	-3.06 ^{a, 17}	-	16.1 ¹⁷	959.8 ¹⁷	0.256 ¹⁷
Carbon disulfide, CS ₂	1.6319 ¹⁷	-8.00 ¹⁷	310-360 ^{b, 19}	0.352 ¹⁷	1255.6 ¹⁷	0.149 ¹⁷

* Except where indicated properties are given at room temperature conditions and measured at 590nm. a = measurement reported at 600nm, b = measurement reported between 530nm and 532nm, c = measurement reported at 1060nm,

2.2. Optofluid Dynamics

On length scales relevant to optofluidic devices (between 10nm and 5mm), fluid flow and species transport can be accomplished using numerous different techniques, a few of which include: traditional pressure driven flow, electrokinetic transport²¹, buoyancy²², magnetohydrodynamics²³, capillarity, electrowetting²⁴ and thermocapillarity²⁵ (see Stone *et al.*²⁶ for a comprehensive overview). In general all flows can be classified as either body force driven (as in the former four of those listed above) and surface force driven (as in the latter three). Although examples exist to the contrary in general body force driven flows have been more successfully exploited in confined channel geometries, whereas free surface techniques are more popular for discrete droplet techniques. It is important to note that this statement is a general trend and by no means a rule (as capillarity, electrowetting and thermal manipulation of surface forces have all been used in channel driven geometries).

In either case fluid motion is governed by the momentum Eq. (2.1a) and continuity equations Eq. (2.1b) shown below,

$$\rho \left(\frac{\partial \mathbf{v}}{\partial t} + \mathbf{v} \cdot \nabla \mathbf{v} \right) = -\nabla p + \eta \nabla^2 \mathbf{v} + \mathbf{f}, \quad (2.1a)$$

$$\nabla \cdot \mathbf{v} = 0, \quad (2.1b)$$

where v , t , p , η , and ρ are velocity, time, pressure, viscosity and density respectively and \mathbf{f} represents an applied body force. Though it is beyond the scope of this paper to provide a comprehensive review of the equations for all transport mechanisms mentioned above we will provide a brief overview of some of those mechanisms which may be most appropriate for optofluidics. Pressure driven flow, for which \mathbf{f} is zero in Eq. (2.1), tends to be the simplest transport mechanism to implement and is accomplished by applying a mechanical pressure difference between an inlet and an outlet port. For the simplest case of pressure driven flow in a microchannel with low aspect ratio it can be shown that the average velocity in the channel is described by Eq. (2.2) below,

$$\mathbf{v}_{ave} = \frac{h^2}{12\eta} \nabla P, \quad (2.2)$$

where h is the channel height. The geometric dependence of velocity shown in Eq. (2.2) represents the most significant weakness of pressure driven fluidics in that as one approaches the nanoscale the flow velocity either becomes debilitatingly small or the required pressure exceedingly high. As will be discussed in section 3.1 one potential solution to this is to perform all major manipulations in a microscale fluidic engine and couple the results to a small nanofluidic network to minimize the flow length at the nanoscale. Alternatively a different transport mechanism can be used which does not exhibit such a fundamental limitation. In electrokinetic transport results from the interaction of an externally applied electric field, $\nabla\phi$, with the net charge density ρ_e , in the electrical double layer (the body force term in Eq. (2.1) becomes $\mathbf{f} = \rho_e \nabla\phi$). The electrical double layer is a very thin region of non-zero net charge density near the interface (in this case a solid-liquid interface) and is generally the result of surface adsorption of a charged species and the resulting rearrangement of the local free ions in solution so as to maintain overall electroneutrality. In general it can be shown that

for electroosmotic flow in a channel with uniform properties Eq. (2.1) reduces to a flat velocity profile (as opposed to the parabolic velocity profile associated with pressure driven flow) whose velocity is described by that below,

$$\mathbf{v}_{ave} = \frac{\varepsilon_w \varepsilon_o \zeta}{\eta} \nabla \phi = \mu_{eo} \nabla \phi \quad (2.3)$$

where μ_{eo} is the electroosmotic mobility and ε_o and ε_w are the dielectric permittivity of a vacuum and the local relative dielectric permittivity (or dielectric constant) of the liquid respectively. In general μ_{eo} is of the order 10^{-4} cm²/Vs and flow velocities on the order of 1mm/s are achievable with applied potential fields of 1000 V/cm. The advantage of electrokinetic flow are that the flow velocity does not scale with channel height (outside the limit of double layer overlap and then only weakly until the extreme cases) and thus is more appropriate for nanoscale fluidics. The most significant disadvantage is that μ_{eo} is highly sensitive to the conditions at the solid liquid interface and is thus only applicable to a limited class of fluids, typically aqueous based solution. Even within this class μ_{eo} is strongly dependent with on ionic concentration and becomes exceedingly small in the high molarity (*i.e.* high refractive index) solutions listed in Table 2.1. Electrokinetics in high molarity solutions also tends to have other difficulties such as joule heating. The coupling of these effects complicates the use of electrokinetics for optofluidic devices.

As mentioned above, the other class of fluidic manipulation of particular interest in optofluidic applications are surface force driven techniques. In such techniques fluidic motion is induced applying an external perturbation to the equilibrium conditions at the interface between two phases. The normal stress conditions at the interface between two phases is described by Eq. (2.4)²⁷.

$$(p - \tau_{nn})_a - (p - \tau_{nn})_b = \sigma \left(\frac{1}{R_1} + \frac{1}{R_2} \right) \quad (2.4)$$

where the subscripts a and b represent the two phases τ_{nn} is the stress normal to the interface, σ is the surface tension and R_1 and R_2 are the principal radii of curvature. The applied perturbation, which most commonly is either electrically (*i.e.* electrowetting), thermally or chemically based, induces a local change in either the surface tension or curvature (often observed as a change in the solid-fluid contact angle) which, from Eq. (2.4), in turn results in a pressure gradient and subsequent motion within at least one of the phases. While such techniques have proven extremely successful for both optical and lab-on-chip type devices, the activation energy required to overcome surface roughness tends to limit such effects to relatively large droplet sizes.

3. Optofluidic Implementation

In this section we will present details of a series of optofluidic projects currently underway within the Center for Optofluidic Integration at the California Institute of Technology. Section 3.1 will describe the integration of nanofluidics with nanophotonics to address and fluidically tune individual features within a photonic crystal. Section 3.2 will summarize our recent work on optofluidic microscopy, creating ultrasmall nanohole imaging devices. Optofluidic distributed feedback dye lasers will be discussed in section 3.3.

3.1. Nanofluidically Tunable Photonic Crystals

While optofluidic integration affords inherent benefits ranging from adaptability to thermal stabilization, some of the most significant advantages lie with the use of nanoscale fluidics to addresses individual elements within a photonic structure at the sub-wavelength level. Photonic crystals²⁸ are attractive for controlling optical propagation by introducing pre-engineered defects into an otherwise regular lattice (to create, for example, waveguides, resonant cavities and filters). While tuning techniques such as mechanical deformation²⁹, thermooptics³⁰, liquid crystal infusion^{4,31} liquid plugs³²⁻³⁴ and others³⁵⁻³⁸ have been developed, at present they rely on modifying the optical properties of the entire crystal. Selective addressing and tuning of individual defects could enable greater functionality than is currently possible. At present most optofluidic devices rely on manipulating optical properties at length scales significantly greater than the wavelength of light. The development of a technique for enabling fluidic addressability at the 100nm scale, however, poses significant challenges in terms of integration, alignment and operation. In this section we will outline our general approach to using soft-lithography³⁹ based nanofluidics to dynamically modulate the index of refraction of targeted defects within a photonic crystal at sub-wavelength length scales. We present a general architecture for the integration of nanofluidics and nanophotonics and experimentally demonstrate the fluidic control of the optical transmission through a single row of

holes in a two dimensional slab silicon-on-insulator photonic crystal. The technique for manufacturing, assembling and operating such devices will also be outlined in detail.

3.1.1. Nanoscale Optofluidic Integration

As mentioned above the integration of fluidics and photonics at the 100 nanometer scale represents a significant challenge in terms of fabrication, alignment and operation. From an operational perspective addressing individual features within a photonic crystal necessitates the use of nanoscale fluidics, however as outlined in Section 2.2 the complex fluidic switching, dispensing and mixing required to operate such devices becomes exceedingly difficult at those length scales. In this section we will begin by describing our general approach to nanoscale optofluidic integration. Fabrication details for the particular case examined here are outlined in Figure 3.1 and will be expanded on throughout this section.

The first level of integration is the nanophotonic level which comprises of the device or devices to be fluidically targeted, defined on the base substrate which also provides support for the fluidics. In this case we use an array of 30 identical photonic crystal structures defined in SOI, each with a triangular lattice of holes constant $a = 434\text{nm}$, hole radius $r = 140\text{nm}$ and height $h = 207\text{nm}$. In the experiments presented here we increase the radius of the holes within the central row of the photonic crystal (which is to be targeted fluidically) to 203nm in order to introduce a reduced index guided mode⁴⁰ into the band gap created by the otherwise regular crystal lattice. This geometry was selected on the basis of a series of numerical experiments as having transmission properties that were most sensitive to changes in index of refraction within the targeted region. A modified approach is used to that described previously⁴¹ in that we defined the

pattern in a negative flowable oxide resist which is left on after processing to enhance bonding with the fluidic layer. Additionally we do not etch the underside insulator layer in favor of using it to enhance the mechanical stability of the structure. In some cases it is also favorable to form an electrically insulating layer over the photonic structure to prevent shorting through the liquid of electrically active photonic devices and similarly to avoid shorting through the photonic structures for electric field driven flows. In general, “flow through” photonic structures (such as membrane suspended photonic crystals) require much more complicated

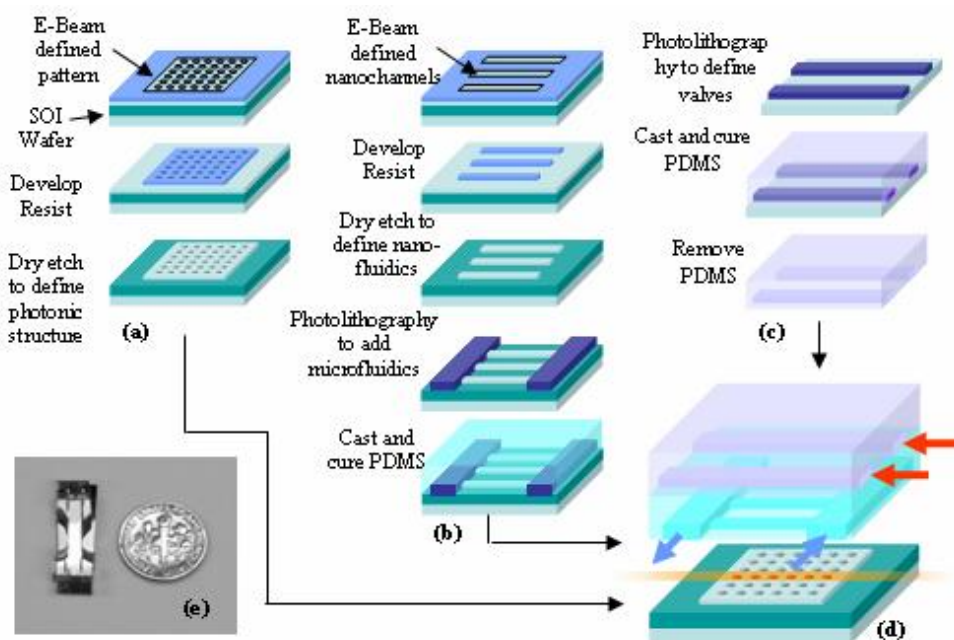


Figure 3.1: Fabrication and assembly procedure (a) Nanophotonic structure (b) Nanofluidics with Microfluidic Coupling (c) Valve control layer (d) Device assembly (e) Photograph of actual Chip.

fluidic confinement schemes on both sides of the device and therefore well type structures are typically preferred (though caution must be observed not to use too high of an aspect ratio to ensure wetting of the device).

The second level of integration is the nanofluidic level which enables direct fluidic coupling into the photonic structure. In this case the nanofluidic system consists of an array of 350nm wide channels spaced with $5\mu\text{m}$ period. The purpose of the nanofluidics level is to provide fluidic coupling between the photonic structure and the upper level of integration

which we refer to as the microfluidics engine. The microfluidics engine structure (with a channel height of $10\mu\text{m}$ and width of $50\mu\text{m}$) is superimposed on the same nanofluidic substrate (in photoresist using standard photolithographic processing). The engine provides the microfluidic functionality, specifically switching and mixing, which can be more conveniently be performed at the 10s of microns length scale.

Figure 3.1 shows a general overview of the fabrication and assembly procedure. As mentioned above the photonic level is fabricated through traditional e-beam lithography and dry etching. Similar processing is used to hard define the nanofluidic structure into a separate SOI substrate. The flow channels of the microfluidics engine structure are then superimposed on the nanofluidic substrate in photoresist ensuring that some overlap exists between the two structures so as to ensure strong fluidic coupling between the two. The master is then cast in RTV elastomer and bonded to a valve control layer which provides the active control. The fluidics were then interfaced and bonded with the photonic structure by placing them in conformal contact after a 7s air plasma oxidation. To align the nanochannels with the targeted row of holes we vary the spacing between the photonic crystals by one half the diameter of the central row of holes. When interfaced with the regularly spaced array of nanochannels, this ensures that at least one nanochannel will be aligned with the central row of at least one photonic crystal. In addition to manufacturing simplicity, building the fluidic layer separately from the optical layer in a soft polymer such as RTV has several inherent advantages including air permeability and the ability to make a conformal seal over the photonic structures.

After assembly, the nanochannels were initially infused with a 1% surfactant solution of Cetyltrimethylammonium bromide (CTAB) in DI water which served to reduce the surface tension at the air liquid interface and facilitate wetting of the nanochannel arrays as shown in Figure 3.2(a-b). Though direct observation of the nanowells during an online experiment was not possible, the repeatability of the experiments presented here suggested that the CTAB solution was sufficient to ensure wetting of the photonic structure as well. The air permeable nature of the RTV fluidics was also likely instrumental in removing air bubbles which may otherwise have been trapped within the system. To directly examine the channel alignment and seal integrity at the nanoscale we conducted an experiment where we initially infused a highly concentrated CTAB solution (roughly 5% by mass) into the fluidic system and allowed the solvent to evaporate overnight. SEM images of the residue after removal of the RTV fluidics are shown in Fig. 3.2d for an aligned channel. As can be seen in the fluid was confined to a single row of holes within the photonic structure. Close examination around the exterior of the photonic crystal shows some residue (more prevalent in the misaligned case) which may be the result of a small leak where the nanochannel first comes in contact with the photonic structure and must conform to the jump interface. As can be seen however this leakage remained confined outside the photonic crystal and does not appear to have significantly affected the targeted delivery.

For this work we selected solutions of aqueous CaCl_2 which, as outlined in section 2.1, ranged in index from DI water, $n = 1.33$, to 5M, $n = 1.45$. Fig. 3.2e shows the normalized quasi-TE mode transmission through the photonic crystal with a fluidically modulated waveguide (i.e. central row aligned with a nanofluidic channel) for DI water and 5M CaCl_2 . The data presented has been smoothed to remove higher frequency Fabry-Perot resonances. The results show a shift in the peak transmission of the guided mode from $a/\lambda = 0.291$ to $a/\lambda = 0.289$ (corresponding to a $\Delta\lambda=15\text{nm}$) when the lower index liquid is displaced by the higher index salt solution. The higher index solution effectively serves to decrease the size of the holes and shifts the guided mode towards the dielectric band of the regular crystal. As can be seen from Fig. 3.2e increasing the index difference between the two fluids would provide a greater shift in the peak transmission of the guided mode, however it would not provide for a significantly higher extinction ratio.

Dynamic modulation of the transmitted power is demonstrated in Fig. 3.2f (and illustrated in Figure 3.2c) at $a/\lambda = 0.291$ by fluidically switching between the DI water and CaCl_2 solutions. As can be seen extinction ratios on the order of 20dB are obtained with a switching speed on the order of 10s of seconds. The modulation speed is inherently limited by the viscous nature of the process. For pressure driven flows we can estimate the timescale for hydrodynamic switching by examining the time required to completely displace one liquid with another from a nanochannel given by $t_{\text{switch}} = 12 \eta L^2 / \Delta P D_h^2$. The applied pressure, ΔP , for this case was between 15 kPa and 30 kPa limited by the sealing stability between the PDMS and the photonic substrate. The channel hydraulic diameter, D_h , is fixed by the photonic geometry. The channel length, L was $400\mu\text{m}$ which could be reduced by at least an order of magnitude resulting in two order of magnitude decrease in the switching time however this is still in the millisecond range.

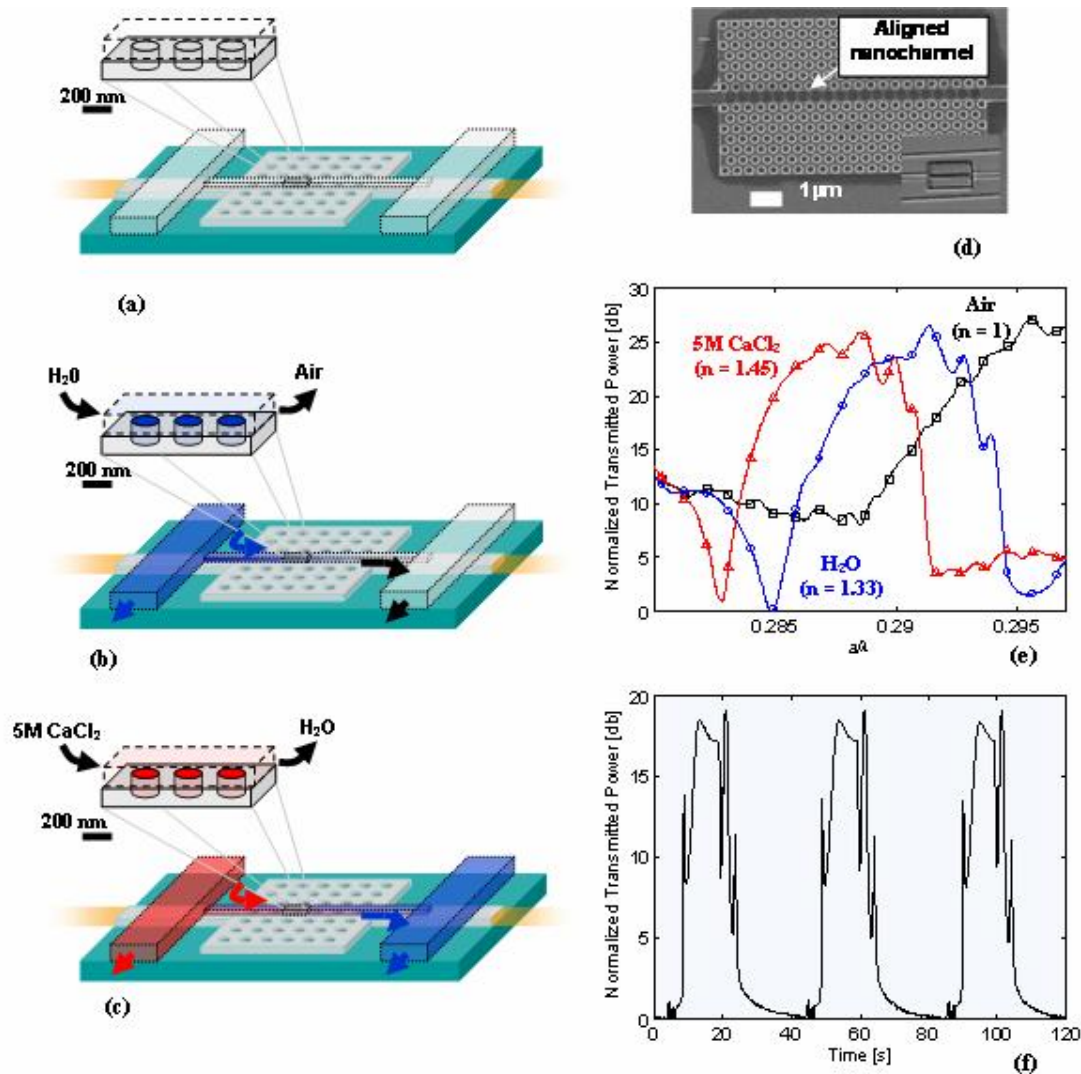


Figure 3.2: Nanofluidic Tuning of Photonic Crystals. (a-c) Stages of operation (a) integration with PDMS fluidics (b) wetting with DI water ($n = 1.33$) (c) displacement of water with 5M CaCl_2 ($n = 1.45$). (d) Nanochannel trace demonstrating subwavelength alignment, sealing and complete infusion of wells. (e) Transmission spectra through photonic crystal for air, water and 5M CaCl_2 (f) Dynamic switching at $a/L = 0.291$ between DI water and 5M CaCl_2 .

3.2. Optofluidic Microscopy

Traditional microfluidics may well be to the first half of the 21st century what microelectronics was to the latter half of the 20th century. The development of the integrated circuit allowed electrical devices to shrink from room-sized to pocket-sized, all the time increasing in speed and penetrating into nearly every aspect of our lives. Similarly, it is hoped that many of the large, expensive chemical and biological analyses currently being performed can be replaced by integrated microfluidic devices, often called labs-on-chip, resulting in a similar revolution. When initially proposed in the early 1990s it was thought that the most significant benefit of these lab-on-chip devices would be the analytical improvements associated with the scaling down of their size however further development revealed other important advantages including: minimized consumption of reagents, increased potential for multistage automation and reduced cost-per-test.

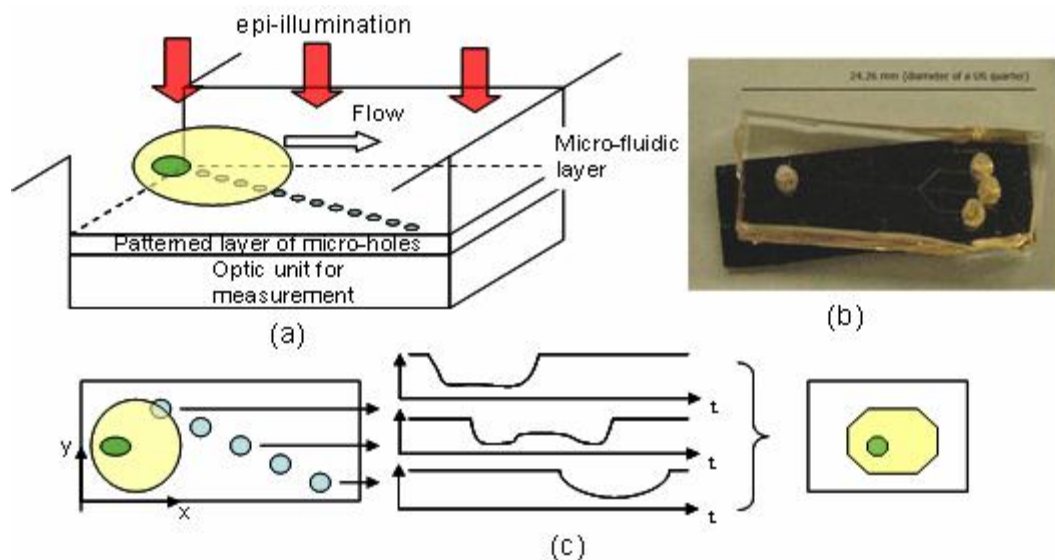


Figure 3.3: Operating principle for the optofluidic microscope. (a) A slanted nanohole array is fashioned in an opaque metal layer in such a way that it spans the width of the imaging microchannel. (b) optical image of the prototype chip. (c) Changes in the transmission through the nanohole array are monitored as a target flows over the imager. By shifting and reconstructing the changes in transmission intensity an image of the target can be constructed.

At present on of the significant hinderences towards the development of fully portable, stand alone lab-on-chip devices, is the reliance on macroscale infrastructure such as pumps, power sources and most importantly external optics which are not particularly amenable to portability. In this project we are developing an integrated optofluidic microscope (OFM) which integrates a high resolution imager, in the form of a slanted nanohole array, directly into the microfluidic network. In this section we will present an overview of the device, details of the fabrication and images of *Chlamydomonas* and *Caenorhabditis elegans* acquired with the prototype chip.

Figure 3.3 provides an overview of the operating procedure for the OFM. The target object is made to flow through the microfluidic channel at a constant velocity using either electrokinetic control or pressure driven flow and confined to the center of the imager through upstream focusing. In the current arrangement the imager consists of a slanted nanohole array defined in an opaque layer (typically aluminum) which spans the width of the channel (fabrication and assembly details provided in the following section). As is shown in the current arrangement the device is epi-illuminated and the transmission through the holes is monitored as the target flows over the imager. For the length of time the target flows over each individual well the transmission is reduced (as shown in Figure 3.3c). Given that the flow rate is known the transmission traces can be used to reconstruct an image of the target. For such an imager the resolution in the direction perpendicular to the flow (which we will define as the x-direction), r_x , is fundamentally limited only by the widthwise spacing between adjacent holes given by

$$r_x = \frac{w}{n_h}, \quad (3.1)$$

where w is the width of the channel and n_h is the number of holes. Since the holes are separated in the lengthwise direction by a distance greater than the diffraction limit n_h can be made arbitrarily small limited only by the resolution of the fabrication technique used to create the holes. In the flow, y , direction the resolution is limited by the transport speed, u , and the frame rate of the acquisition device, fps , as described by Eq. (3.2)

$$r_y = \frac{u}{fps} = \frac{L_y}{\Delta t} \frac{1}{fps}, \quad (3.2)$$

Where L_y is the length of the imager in the y direction and Δt is the length of time required for the target to be transported over the array. In this latter case if the target flow speed is $100 \mu\text{m/s}$, and the detector's reading rate is 1 KHz , the maximum resolution in the x direction would be equal to 0.1 micron . Both these ultimate resolutions are practically limited by the stability (in terms of, for example, tumbling and Brownian diffusion) of the target as it passes over the imaging array. For electrokinetic flows where the flow profile is pluglike and does not exhibit significant velocity gradients outside the double layer, tumbling should be minimized. The loss of resolution due to Brownian diffusion is governed by the expected diffusion distance during the course of an imaging operation and is proportional to the square root of the target diffusion coefficient and the time over the imaging array. While the diffusion coefficient is fixed by the target to be imaged, reducing increasing the flow rate to reduce the Brownian drift, conflicts with the y-direction resolution from Eq. (3.2). As such there should exist an optimal flow speed for imaging at which the highest resolution is achieved.

Fabrication of the device begins by depositing an opaque metal layer (Au or Al) on ultraclean glass substrate. Next, a slanted nanohole array is patterned on PMMA 495 by E beam lithography (Leica VB6) and transferred onto metal layer by dry etching or ion milling. The microfluidic system is fabricated in RTV elastomer, as described previously, and then aligned and bonded with the imaging substrate such that it fills the entire width of the micro channel. The microfluidic circuitry is accomplished by replica molding with PDMS.

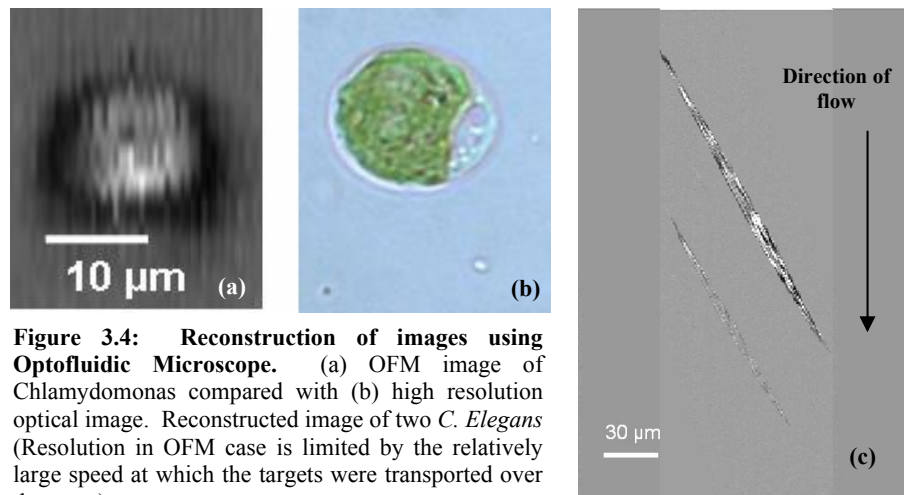


Figure 3.4: Reconstruction of images using Optofluidic Microscope. (a) OFM image of Chlamydomonas compared with (b) high resolution optical image. Reconstructed image of two *C. Elegans* (Resolution in OFM case is limited by the relatively large speed at which the targets were transported over the array).

As mentioned above we have successfully imaged several different biological species with the initial prototype and here we will present some initial proof of concept images of chlamydomonas and *C. elegans*. Figure 3.4(a) shows an image of a single chlamydomona taken with the OFM and compared with a high resolution optical image (b). In this case flow was generated by a slight difference in pressure head between the upstream and downstream reservoirs and a focusing fluidic geometry was used to guide the cell over the center of the imaging array. As can be seen roughly the correct size and shape of the cell are extracted. Figure 3.4(b) shows a similar OFM image taken of two *C. Elegans*. In these experiments a syringe pump was used to transport the targets over the array at a rate of approximately 1.57 mm/s yielding a relatively large resolution size in the y direction of $3.4 \mu\text{m}$. As in the previous case the correct shape and size of the target is extracted which should be sufficient for high speed phenotyping.

3.3. Optofluidic Dye Lasers

At the onset of modern microfluidics in the early 1990's glasses, quartz and silicon were the materials of choice for microfabrication, primarily due to the well established wet etching and lithography based micromachining techniques developed by the electronics and semiconductor industries. While both silicon and

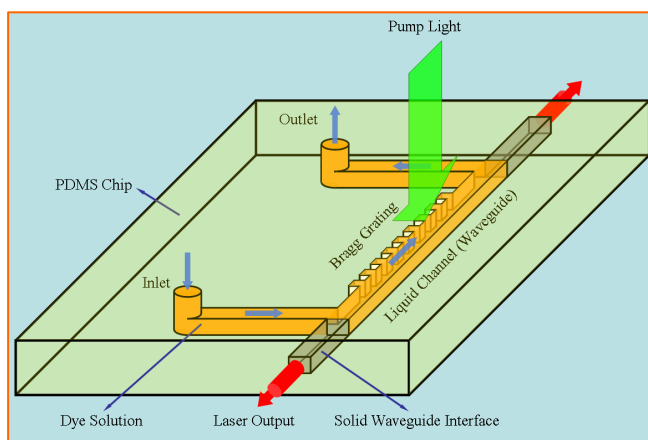


Figure 3.5: Schematic of an optofluidic Distributed Feedback (DFB) dye laser.

glass based microfabrication techniques proved extremely successful for building a variety of microfluidic devices, in general they have the drawback of being expensive (on the order of \$4000/m² for glass being the cheaper of the two) and time consuming (the fabrication processes themselves require a long time as well as the training required for new fabricators to gain a sufficient skill level). Additionally, stringent bonding requirements (in terms of substrate flatness and material compatibility as well as the thermal conditions associated with the bonding process itself) can make it difficult to integrate higher level components and biological entities into such devices. As a result of these difficulties

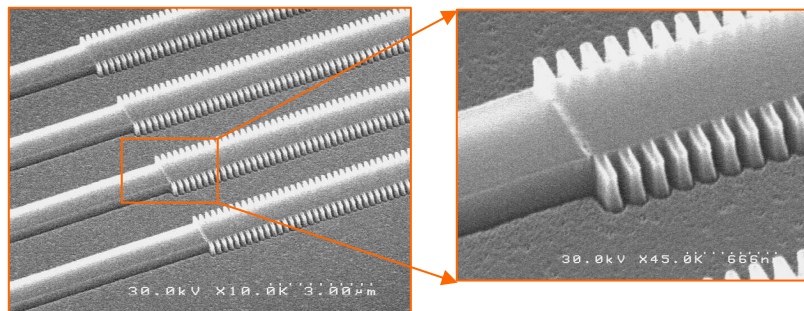


Figure 3.6: Scanning electron microscope image of an array of silicon molds for the first order DFB structure. Grating period is 200nm. The width and height of the waveguide are 1µm and 250nm respectively.

with traditional microfabrication materials and techniques, there has been a recent thrust to manufacture microfluidic systems and biochips from low-cost polymeric materials primarily poly(dimethylsiloxane) (PDMS). As a result of this widespread adoption of PDMS as a material of choice for microfluidic systems, there has been a large thrust towards creating structures which can be easily cast into the soft elastomer fluidics and provide more advanced functionality.

Organic dye lasers use dye molecules dissolved in solvents as gain media. The broad emission spectra of dye molecules enables both continuously tunable laser output and ultra-short pulse generation. In addition, there are over 200 laser dyes available that when used sequentially can produce laser emission from 320nm to 1200nm⁴². In this section we will review our recent work on the development of horizontal emission distributed feedback dye lasers fabricated entirely in PDMS. Such lasers would be of great interest for on-chip spectroscopy and cell sorting applications. In this section we will detail the fabrication procedure for our laser and summarize our initial higher order lasing results.

3.3.1. Principles and Fabrication

Distributed feedback (DFB) cavities combined with 3D optical waveguides are very efficient structures for making single frequency microfabricated lasers as has been demonstrated in semiconductor lasers. We also use these structures for the optofluidic dye lasers as shown in Figure 3.5. In our implementation, a solution of Rhodamine 6G lasing dye in a Methanol, Ethylene Glycol solution is introduced into a microfluidic channel. The refractive index of the solution (n = 1.42) is slightly higher than that of PDMS (1.406) at visible wavelengths so that the dye solution and PDMS act as the core and the cladding of an optical waveguide respectively. To provide the feedback mechanism, a Bragg grating is fabricated on the sidewall of the channel. To obtain single frequency operation, a λ/4 phase shift is added at the center of the grating. The lasing wavelength is given by the relation:

$$\lambda = 2n_{eff}\Lambda \quad (3.3)$$

where, λ is the lasing wavelength, n_{eff} is the effective index of the guided mode, Λ is the period of the grating. Tunable laser output can be obtained by either changing the index of the dye solution or mechanically varying the grating period.

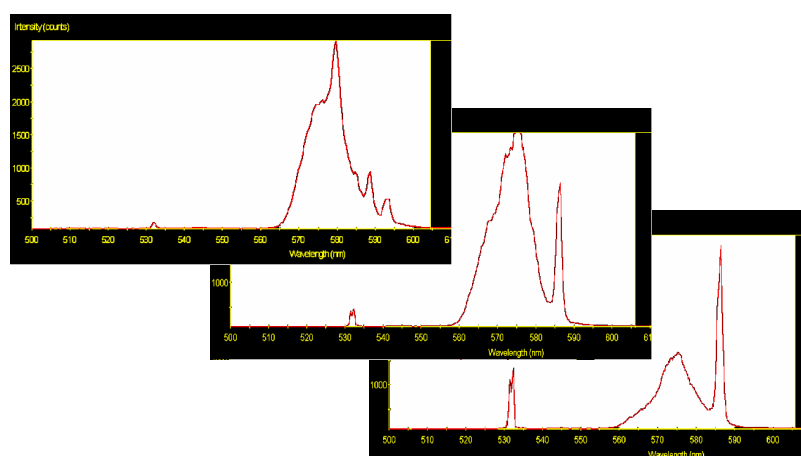


Figure 3.7: Emission spectra of an optofluidic DFB dye laser using a higher-order DFB structure. Images show increase in lasing peak with optical pumping power.

As mentioned above the laser chip is fabricated using soft lithography using traditional replica molding using a similar technique to that described in section 3.1. Figure 3.6 shows a scanning electron microscope image of an array of silicon masters for the first order DFB structure fabricated using E-beam lithography and dry etching. The grating period is ~200nm which corresponds to ~565nm lasing wavelength for a dye solution with refractive index 1.42.

3.3.2. Results

As is demonstrated in Figure 3.7, we have achieved lasing at 585nm using a higher-order (~100th order) DFB structure using our initial prototype device fabricated using traditional photolithography. For this case the grating period was 20um (free spectral range ~ 6nm) which leads to multiple frequency lasing at low pumping levels. The dye solution was pumped by 6ns 532nm Nd:YAG laser pulses. The pump laser beam was focused to a 200um by 5mm stripe on the channel. The threshold pump fluence is about 10mJ/cm².

4. SUMMARY

“Optofluidics” represents a new approach for dynamic manipulation of optical properties at length scales both greater than and smaller than the wavelength of light with applications ranging from reconfigurable photonic circuits to fluidically adaptive optics to high sensitivity bio-detection currently under development. We have discussed some of the fundamental fluidic and optical issues related to optofluidic integration and demonstrated three classes of devices.

REFERENCES

1. Gibson, B., Liquid Mirror Telescopes: History. *J. Royal. Astron. Soc. Can.* 85 158-171 (1991)
2. Whitesides, G., Stroock, A., Flexible methods for microfluidics. *Physics Today*, 54, 42-48 (2001).
3. Thorsen, T., Maerkl, S., Quake, S. *Microfluidic Large Scale Integration Science* 298, 580-584 (2002).
4. Maune, B. Lonkar M., Witzens J., Hochberg M., Baehr-Jones, T., Psaltis, D., Scherer, A., Qiu Y. Liquid-crystal electric tuning of a photonic crystal laser. *App. Phys. Lett.* 85 360-362 (2004).
5. Wolfe, D., Conroy R., Garstecki, P., Mayers, B., Fischbach, M., Paul, K., Prentiss, M., Whitesides, G., Dynamic control of liquid-core liquid-cladding optical waveguides. *PNAS* 101 12434-12438 (2004).
6. Vezenov, D., Mayers, B., Wolfe, D., Whitesides, G. Integrated fluorescent light source for optofluidic applications. *Appl. Phys. Lett.* 86 041104 (2005)
7. Campbell, K., Groisman, A., Levy, U., Pang, L., Mookherjee, S., Psaltis, D., Fainman, Y. A microfluidic 2x2 optical switch. *App. Phys. Lett.*, 85, 6119-6121 (2004).
8. Mach, P., Dolinski, M., Baldwin, K., Rogers, J., Kerbage, C., Windeler, C., Eggleton, B. Tunable microfluidic optical fiber. *Appl. Phys. Lett.* 80, 4294-4296 (2002).
9. Cattaneo, F., Baldwin, K., Yang, S., Krupenkine, T., Ramachandran, S., Rogers, J. Digitally tunable microfluidic optical fiber devices *J. MEMS* 12, 907-912 (2003).
10. Domachuk, P., Grillet, C., Ta'eed, V., Magi, E., Bolger, J., Eggleton, B., Rodd, L., Cooper-White, J. Microfluidic interferometer. *Appl. Phys. Lett.* 86 024103 (2005).
11. Kuiper, S., Hendriks, B., Variable-focus liquid lens for miniature cameras. *Appl. Phys. Lett.* 85, 1128-1129 (2004).
12. Hayes, R., Feenstra, B. Video-speed electronic paper based on electrowetting *Nature* 425, 383-385 (2003)
13. Yano, M., Yamagishi, F., Tsuda, T. Optical MEMS for photonic switching-compact and stable optical crossconnect switches for simple, fast, and flexible wavelength applications in recent photonic networks. *IEEE J. Quantum Elec.* 11 383-394 (2005)
14. Prasad, P. *Introduction to Biophotonics*, John Wiley and Sons, New Jersey (2003)
15. Erickson, D., Li, D., Integrated microfluidic devices. *Anal. Chim. Acta.* 507 11-26 (2004)
16. Vahala, K., Optical Microcavities. *Nature* 424, 839-846 (2003).
17. Weber, M. *Handbook of Optical Materials*, CRC Press, Florida (2003)
18. Lide, D. (Ed.) *Handbook of Chemistry and Physics*. CRC Press (1982).
19. Sutherland, R., *Handbook of non-linear optics* 2nd Ed. Marcel Dekker, New York (2003)
20. Lee, J., Park, C., Whitesides, G., Solvent Compatibility of Poly(dimethylsiloxane)-Based Microfluidic Devices. *Anal. Chem.* 75 6544-6554 (2003).
21. Hunter, R. *Zeta potential in Colloid Science*, Academic Press, London, 1981
22. Krishnan N, Agrawal N, Burns MA, Ugaz VM Reactions and fluidics in miniaturized natural convection systems. *Anal. Chem.* 76, 6254-6265 (2004)
23. Xiang, Y., Bau, H. Complex magnetohydrodynamic low-Reynolds-number flows. *Phys. Rev. E* 68 016312 (2003)
24. Zeng, J., Korsmeyer, T., Principles of droplet electrohydrodynamics for lab-on-a-chip. *Lab Chip* 4, 265-277 (2004)

25. Darhuber AA, Valentino JP, Troian SM, Wagner S Thermocapillary actuation of droplets on chemically patterned surfaces by programmable microheater arrays. *J. MEMS.* 12 873-879 (2003).
26. Stone HA, Stroock AD, Ajdari A Engineering flows in small devices: Microfluidics toward a lab-on-a-chip *Ann. Rev. Fluid. Mech.* 36 381-411 (2004)
27. Panton, R. *Incompressible Flow.* John Wiley and Sons, New York, 1996
28. Joannopoulos, J., Meade, R., Winn, J., *Photonic Crystals: Molding the Flow of Light.* Princeton University Press, Princeton, New Jersey (1995).
29. Park, W., Lee, J-B., Mechanically tunable photonic crystal structure. *App. Phys. Lett.* 85, 4845-4847 (2004).
30. Chong, H., De La Rue, R., Tuning of Photoic Crystal Waveguide by Thermooptic Effect. *IEEE Photonics Tech. Lett.* 16 1528-1530 (2004).
31. Leonard, S., Mondia, J., van Driel, H., Toader, O., John, S., Busch, K., Birner, A., Gosele, U., Lehmann, V., Tunable two-dimensional photonic crystals using liquid-crystal infiltration. *Phys. Rev. B* 61 2389-2392 (2005)
32. Kerbage, C., Windeler, R.S., Eggleton, B.J., Mach, P., Dolinski, M., Rogers, J. Tunable devices based on dynamic positioning of micro-fluids in microstructured optical fiber. *Opt. Commun.* 204, 179-184 (2002).
33. Mach, P., Dolinski, M., Baldwin, K., Rogers, J., Kerbage, C., Windeler, C., Eggleton, B. Tunable microfluidic optical fiber. *Appl. Phys. Lett.* 80, 4294-4296 (2002).
34. Cattaneo, F., Baldwin, K., Yang, S., Krupenkine, T., Ramachandran, S., Rogers, J. Digitally tunable microfluidic optical fiber devices *J. MEMS* 12, 907-912 (2003).
35. Raineri, F., Cojocar, C., Raj, R., Monnier, P., Levenson, A., Seassal, C., Letartre, X., Viktorovitch, P., Tuning a two-dimensional photonic crystal via optical carrier injection. *Opt Lett.* 30, 64-66 (2005).
36. Tan, H., van Driel, H.M., Schweizer, S., Wehrspohn, R., Gosele, U., Nonlinear optical tuning of a two-dimensional silicon photonic crystal. *Phys. Rev. B* 70 205110 (2004)
37. Iwamoto, S., Arakawa, Y., Photonic Crystal with Advanced Micro/Nano-Structures: Quantum Dots and MEMS. *IEICE Trans. Electron.* E87 343-350 (2004)
38. Wild, B., Ferrini, R., Houdre, R., Mulot, M., Anand, S., Smith, C. Temperature tuning of optical properties of planar photonic crystal microcavities. *Appl. Phys. Lett.* 84 846-848 (2004).
39. Duffy, D., McDonald, J., Schueller, O., Whitesides, G., Rapid prototyping of microfluidic systems in poly(dimethylsiloxane). *Anal. Chem.* 70 4974-4984 (1998).
40. Johnson, S., Villeneuve, P., Fan, S., Joannopoulos, J., Linear waveguides in photonic-crystal slabs. *Phys. Rev. B.* 62, 8212 (2000)
41. Loncar, M., Nedeljkovic, D., Doll, T., Vuckovic, J., Scherer, A., Pearsall, T., Waveguiding in planar photonic crystals. *App Phys Lett.* 77, 1937-1939 (2000).
42. Schafer, F., *Dye Lasers.* Springer-Verlag (1990).
43. Xia YN, Whitesides GM, Soft lithography, *Ann. Rev. Mat. Sci.* 28 153-184, (1998).